1st International Conference on Meteorology and Air/Sea Interaction of the Coastal Zone, May 10-14, 1982, The Hague, Netherlands

CHARACTERIZING COASTAL ATMOSPHERIC DIFFUSION FROM THREE-DIMENSIONAL MONITORING OF SF_6 RELEASES

Paolo Zannetti and
David M. Wilbur

AeroVironment Inc.
Pasadena, California

Gordon E. Schacher

Naval Postgraduate School
Monterey, California

1. INTRODUCTION

The need for this study originated from U.S. air quality regulations requiring prediction of environmental impacts for new offshore emission sources. These impacts are predicted by air quality numerical simulation models. However, nearly all available numerical models have been defined (and calibrated) to simulate dispersion over land (e.g., see EPA Guidelines on air pollution modeling; U.S. EPA, 1980). Large bodies of water, due to their smooth surface and especially their greater thermal capacity, than that of land, strongly affect dispersion characteristics and make numerical simulation of diffusion even more complex.

The most important objective of our study has been to evaluate the Gaussian steady-state plume formula. This simple algorithm has been widely used to meet regulatory requirements in the U.S. even though, at least theoretically, this methodology should be applied only to simple homogeneous and stationary short-range dispersion conditions in flat terrain. It was very important to determine if and how the Gaussian formula could simulate tracer dispersion characterized by non-stationary coastal meteorological effects (e.g., the turning of the wind direction) and interaction over non-homogeneous surfaces (e.g., the change at the land/sea interface).

The basic program involved:

1. Field tracer experiments to obtain meteorological and dispersion data over water and at the land/sea interface.
2. Data processing to provide hourly-averaged values of tracer plume concentration distribution and meteorological parameters.
3. Analysis of the tracer plume data to determine Gaussian plume parameters, σ_y and σ_z, for each hour.
4. Analysis of the ability of various stability classification schemes to represent dispersion actually encountered.
5. Validation of Gaussian dispersion models.

In order to evaluate any seasonal difference in dispersion conditions, we performed two tracer dispersion experiments -- one typical of summer conditions (September 24, 27, 28, and 29, 1980) and one typical of winter (January 6, 9, 13, and 15, 1981) -- to cover most possible dispersion conditions in the study area.

The study area included the offshore and inland areas near Ventura, California (about 60 miles northwest of Los Angeles). The tracer gas, SF_6, was released a few miles offshore by the research vessel RV/Acania, a ship supplied by the Naval Postgraduate School (NPS). Tracer gas samples were collected by both fixed and mobile samplers at the surface and aloft to define both the vertical and horizontal distribution of the gas from the release vessel to the shoreline and inland approximately three to five miles. The sampling network is shown in Figure 1.

An aircraft equipped with a continuous SF_6 analyzer was used to profile the plume aloft. Multiple crosswind traverses were flown through the plume at varying altitudes, from as near the surface as possible to the top of the plume, at three locations: (1) approximately one-half mile offshore, (2) approximately one-half mile inland, and (3) three to five miles inland.

A van equipped with another SF_6 continuous analyzer transected the tracer gas plume at approximately one-quarter to one-half-mile inland. Twenty sequential samplers were deployed in arrays (as shown by numbers in Figure 1). These sequential samplers collected six one-hour samples during each study day. In addition, syringe (grab) samples were taken from a boat approximately one-half mile offshore, from a second van approximately three to five miles inland, from the continuous gas chromatograph-equipped aircraft, and from tethersonde locations.

The meteorological measurement network is also shown in Figure 1. Meteorological data were collected from a 10-meter tower (measuring wind speed, wind direction, σ_θ, and σ_w), aircraft, tethersonde and airsonde soundings, and a Doppler acoustic sounder. Aircraft soundings were generally performed over Oxnard Airport and over the water near the RV/Acania, as shown in Figure 1. Additional soundings were performed near the Ventura Marina, approximately one-half mile offshore. A more detailed discussion of the field program of this study can be found in Zannetti et al. (1981).

2. EVALUATION AND CATEGORIZATION OF SIGMA PARAMETERS FROM TRACER DATA

The field data were processed to obtain hourly averages of tracer plume concentrations. SF_6 concentrations were measured by a continuous analyzer in an aircraft, by a continuous analyzer in a van, and by fixed stations and grab sampling. Each type of measurement provided, at each hour, estimates of hourly average plume concentration distributions at different downwind distances, x*, and elevations, z*.

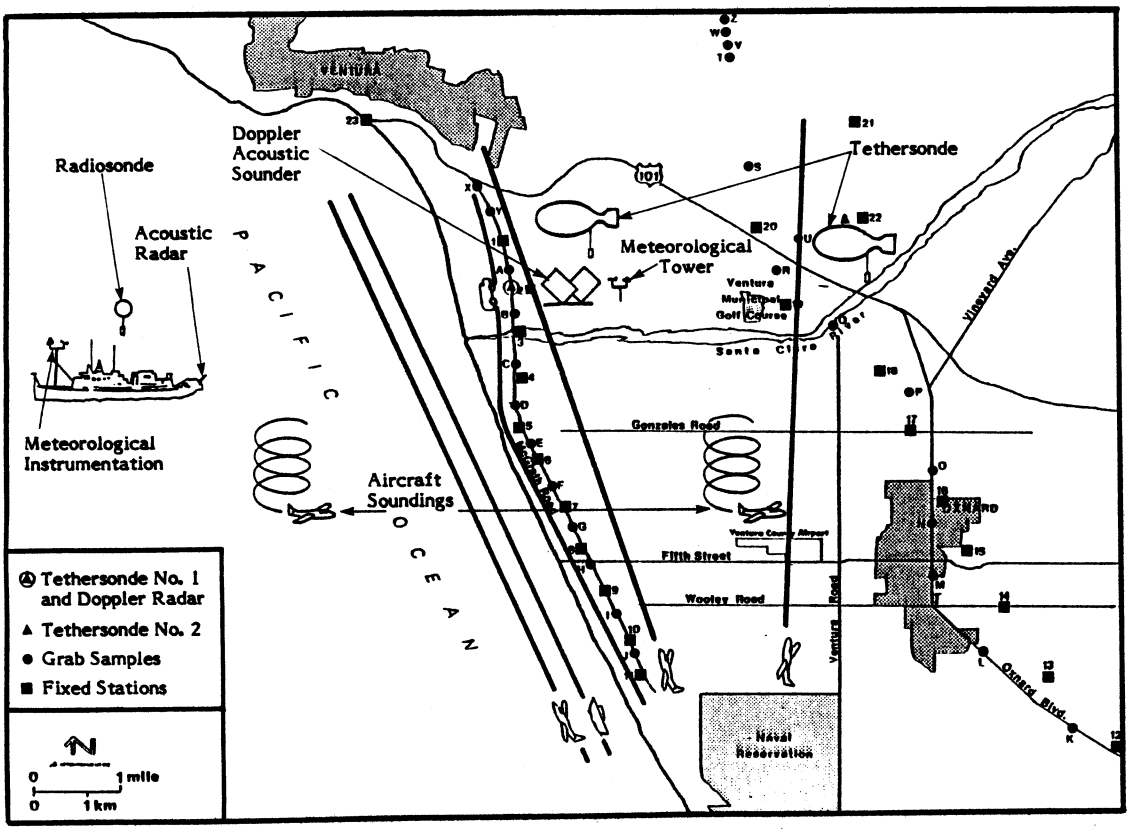

Figure 1. Map showing meteorological and tracer sampling network. RV/Acania was anchored about 9 kilometers offshore.

Fixed stations and grab sampling locations were not evenly spaced across the plume. Therefore, such measurements were projected on a crosswind segment perpendicular to the wind and then linearly interpolated to provide equally-spaced data. Van and aircraft measurements (equally-spaced along the plume transect) provided "instantaneous" plume transects, several of which were averaged to estimate the hourly distribution. Then, all concentrations were projected on the y-axes normal to the plume centerline. In this way, at each hour for each instrument platform, we estimated the hourly averaged crosswind profile of a plume.

2.1 Sigma (σ) Computation

The hourly averaged tracer plume concentration distributions for each hour were analyzed to determine the Gaussian distribution parameters of σ_y and σ_z. Using the hourly crosswind horizontal plume profiles, it was relatively straightforward to calculate $\sigma_y(x^*)$ at each downwind distance, x^*.

To derive $\sigma_z(x^*)$ we required conservation of mass. Using the maximum concentration value of each horizontal transect, available emission (Q) and wind speed (u) data, and the previously computed value $\sigma_y(x^*)$, a nonlinear equation was found for σ_z and, solving this nonlinear equation with an iterative method (secant formula, Dahlquist et al., 1974), three different computational cases were found:

- no real solution for $\sigma_z(x^*)$ (for $z^* > 0$)
- one real solution for $\sigma_z(x^*)$ (always for $z^* = 0$)
- two real solutions for $\sigma_z(x^*)$ (for $z^* > 0$)

The first case means that we have mass balance problems. The third case is due to ground reflection (it disappears at $z^* = 0$) and it was easy, in nearly all cases, to eliminate the spurious solution.

Multiple reflections from terrain and the bottom of an elevated inversion layer (at altitude H_i) could have been considered by simple changes in the steady-state Gaussian equation. However, we considered only the ground reflection for a number of reasons.

The first is that, using multiple reflections, we have more than two multiple solutions for $\sigma_z(x^*)$. Second, our information on the mixing depth, H_i, in spite of our relatively sophisticated data base, is very approximate and the structure of the atmospheric layer during both experiments is extremely complex. Finally, the most recent guidelines on air pollution modeling (e.g., Hanna et al., 1977) suggest forcing σ_z to remain lower than the mixing depth, H_i, strongly reducing the importance of multiple reflection terms.

An additional independent computation of σ_z was possible when aircraft data were available at the same downwind distance x^* at different elevations, z^*. In such a case, $\sigma_z(x^*)$ values have been estimated by considering the vertical profile of the maximum concentration, $C_o(z)$, which, according to the Gaussian equation for the case of effective height of release $H = 0$ (which is practically true in our case), has a half-Gaussian distribution over $z \geq 0$.

Note that in this latter computation we use only the maximum concentration value at each altitude even though its horizontal location can differ with the

altitude due to wind shear effects. This prevents systematic errors in $\sigma_z(x^*)$ computations due to the presence of wind shear during our experiment.

In addition in many regulatory applications we really need only a good estimate of the product $\sigma_y \sigma_z$, since this value allows computation of maximum ground-level ($z^* = 0$) concentration $C_o(0)$ at different downwind distances x^*. In fact, the Gaussian formula for $H = 0$, $z^* = 0$, and zero crosswind distance is:

$$C_o(0) = \frac{Q}{\pi \sigma_y(x^*)\, \sigma_z(x^*)\, u} \qquad (1)$$

Therefore, at each downwind distance x^* where some estimate of the maximum ground-level concentration $C_o(0)$ is available, an estimate of the product $\sigma_y \sigma_z$ can be obtained by simply using Equation (1).

From the above computations, we have a data set of hourly-averaged values of σ_y and σ_z. We have found that, for our data set, σ_y values cover the entire Pasquill-Gifford-Turner (PGT) σ_y range (A through F), while σ_z values are in the neutral to stable range (PGT D-E-F), with a tendency toward lower σ_z values during the second experiment (winter dispersion).

2.2 Sigma (σ) Characterization by Atmospheric Stability

We next analyzed the ability of various stability schemes to represent the dispersion we actually encountered. Analyzing tracer data from an empirical point of view, we can say that the most appropriate stability classification is one that allows the best differentiation in σ_y and/or σ_z behavior as a function of the downwind distance from the source. In other words, we expect a good stability classification scheme to be able to discriminate between high σ values (unstable conditions) and low σ values (stable conditions), even though a large scatter can be tolerated in our experimental data.

For each hour of both experiments, we estimated the stability class using seven different schemes.

1. σ_θ measurements at the RV/Acania;
2. $\Delta T/\Delta z$ surface layer measurements by tethersonde at the shoreline;
3. NPS scheme (briefly discussed in the appendix);
4. σ_θ measurements near the shoreline (only during the second experiment);
5. σ_w measurements near the shoreline (only during the second experiment);
6. $\Delta T/\Delta z$ measurements inland;
7. Standard Pasquill-Gifford (insolation) method using meteorological data collected at the Ventura County Airport.

Looking at this data set of stability classes by the various classification schemes, we conclude first that the different stability classification schemes do not agree, as was also pointed out by Skagg and Robinson (1976), Weil (1979), and DeMarrais (1978). This can be expected since the different schemes define different atmospheric properties, and different manifestations of the effect of turbulence. This exercise, however, gives us an opportunity to test how well σ_y and σ_z values determined from the SF_6 data can be segregated under different stability classification schemes.

In fact, separate plots of σ_y and σ_z versus downwind distance for each stability class and each stability scheme indicate the following:

- No stability classification method is good for both σ_y and σ_z, which seems to confirm that horizontal and vertical dispersion characteristics in our experiments are not strongly interdependent;
- σ_θ at the release point is the best measurement to classify σ_y, as we would expect from the physics of the phenomenon and previous studies (Taylor, 1921; Hanna et al., 1977);
- $\Delta T/\Delta z$ near the shoreline, the NPS method, and the standard Pasquill-Gifford (insolation) method, provide fairly good classification of σ_z, with the $\Delta T/\Delta z$ method being slightly better than the others. From a theoretical point of view, we think the NPS method is best to characterize dispersion over water; however, more empirical analysis is probably needed to calibrate this algorithm for a better σ_y and σ_z classification.

In spite of the large scatter (characteristic of all similar experiments), we feel these results are fairly good, since variations in sigma averages are consistent with the physics of the phenomenon (higher average σ for unstable conditions and vice-versa), and show some agreement with other recent studies of coastal dispersion (e.g., Caltech tracer studies by Reible and Shair, personal communication).

As far as the product $\sigma_y \sigma_z$ is concerned, we found, with some surprise, that the simple (and easily applicable) Pasquill-Gifford insolation method provides a reasonable classification for $\sigma_y \sigma_z$. This is very important for regulatory purposes, where 1) only maximum ground-level concentrations are important, and 2) sometimes only Pasquill-Gifford (insolation) stability values are available since σ_θ and $\Delta T/\Delta z$ measurements over water are not common. However, since the second experiment showed higher maximum ground-level concentrations and lower mixing heights (thus limiting vertical mixing more), we tried to account for this by increasing the stability of the second experiment by one class.

2.3 Empirical Stability Corrections to Fit σ Measurements

From the results of these analyses, we developed a modified dispersion modeling approach, involving a new combined method of stability classification and a new method of relating these stability classes to the standard PGT dispersion curves. σ_θ and $\Delta T/\Delta z$ measurements were selected as most appropriate to determine horizontal and vertical atmospheric stability, respectively, to simulate a three-dimensional plume. The standard Pasquill-Gifford (insolation) method, with an empirical increase by one (more stable) class during winter, was also selected as giving a reasonable, easy to obtain, estimate of general diffusion (both horizontal and vertical) to simulate maximum ground-level concentration only.

However, our average empirical σ values for each stability class did not correspond to the σ values of the Pasquill-Gifford-Turner (PGT) σ, or any other reference dispersion curves. Therefore, some empirical modifications were required; two different approaches were possible:

1. We could define our empirical $\sigma(x^*)$ functions for each stability class, representing the best fit of our experimental σ values, or
2. We could define an empirical correction of stability data in order to make the PGT σ (the most used σ set in regulatory applications) fit our experimental σ.

We chose the second solution for several reasons. First, there are already enough σ formulas in the literature, and defining a new set of curves would require analyzing many more tracer experiments done under similar conditions. Second, using existing available Gaussian computer codes, it is much easier to modify the stability input than the σ curves. Thus, accepting PGT σ, we minimize computer code modifications for future applications of our results.

We have, therefore, empirically defined three conversion tables that, from the measured stabilities, allow the evaluation of the "effective" stability which, using PGT σ, best fits our empirical sigma values.

Tables 1 and 2 show these empirical conversions for each downwind location (offshore, shoreline, inland) for horizontal and vertical stability, respectively.

Table 1
Modification of Pasquill stability classes to best characterize the horizontal shape of the plume.

Measured Stability from σ_θ	"Effective" Horizontal Stability		
	1/2 mile Offshore	1/2 mile Inland	3 to 5 miles Inland
C	B	B	B
D	C-D	B-C	B
E	C	C	C
F	D	C-D	C

Table 2
Modification of Pasquill stability classes to best characterize the vertical shape of the plume.

Measured Stability from $\Delta T/\Delta z$	"Effective" Vertical Stability		
	1/2 mile Offshore	1/2 mile Inland	3 to 5 miles Inland
A	D	D	D
D	F	E	E
E	G	E-F	D-E

In these conversion tables the presence of a couple (e.g., C-D) of classes means that intermediate σ values should be used. The Class G means extremely stable conditions, and its relative σ_z has been estimated by $\sigma_z = 0.32\, x^{*-0.50}$. Tables 1 and 2 show the conversion mechanism for only those stabilities occurring at least a few times during either experiment.

We note that, in general, the effective horizontal stability is lower (more unstable) than measured, while the effective vertical stability is higher (more stable) than measured, again showing a clear degree of independence of one phenomenon with respect to the other.

Table 3 shows the empirical conversion mechanism for the "general" stability used for addressing only the maximum ground-level concentration problem.

Table 3
Modification of Pasquill stability classes for computing ground-level maximum concentration.

Pasquill-Gifford Computed Stability Class*	Effective Stability
B	D
C	D
D	D
E	D-E
F	E

*One class more stable for winter

3. GAUSSIAN MODEL VALIDATION

Our final step was to perform dispersion model validation on our modified modeling approaches. No real validation has been possible since an independent data set was not available. However, using the same data used for estimating σ, some meaningful performance evaluation of our σ classification methods has been possible.

Two types of Gaussian modeling approaches were validated. The first was the standard three-dimensional Gaussian (G3D) steady-state equation, where σ_y and σ_z were computed using the PGT curves with the horizontal and vertical atmospheric stability computed, respectively, by σ_θ (and Table 1) and $\Delta T/\Delta z$ (and Table 2) measurements. The second validation (GMAX) consisted only of computing maximum ground-level concentration using PGT σ curves and atmospheric stabilities computed by the Pasquill-Gifford (insolation) method (and Table 3). Validation consisted of computing concentration values at each hour at each original monitoring point, forcing the maximum computed concentration to be in the same y-location (crosswind) as the maximum measured concentration at any downwind distance and any elevation.

3.1 G3D Model Validation

Table 4 summarizes the principal statistical characteristics of such comparisons, viz., the average measured concentration, the average computed concentration, the median and the average of the absolute error between each couple of concentrations (measured-computed) at the same point, their correlation coefficient, and the regression line parameters.

Table 4

Gaussian model comparison statistics for each type of measurement and each experiment.

Type of Measurement	Experiment*	Average Measured	Average Computed	Absolute Error		Correlation Coefficient	Regression Line	
				Median	Average		Slope	Intercept
Van	1	968	1,065	375	454	0.70	0.60	474
	2	1,219	833	607	734	0.55	0.30	517
Fixed	1	358	389	150	274	0.78	0.80	109
	2	521	420	173	365	0.62	0.40	215
Air	1	355	111	152	250	0.47	0.10	66
	2	756	814	318	451	0.80	0.80	197

*1 = summer; 2 = winter

Table 5

Gaussian model comparison statistics for maximum ground-level concentration (see text for full explanation of numbers between parentheses).

	Average Measured	Average Computed	Absolute Error		Correlation Coefficient	Regression Line	
			Median	Average		Slope	Intercept
Experiment 1 (Summer)	(1,801)*	(1,650)	(500)	(599)	(0.70)	(0.50)	(827)
	1,574	1,217	375	673	0.64	0.30	778
	(1,574)	(657)	(1,000)	(1,198)	(0.05)	0.00	614
Experiment 2 (Winter)	(2,067)*	(1,166)	(875)	(1,117)	(0.63)	(0.20)	(698)
	1,870	2,017	475	862	0.52	0.30	1,474
	(1,870)	(1,231)	(750)	(966)	(0.57)	(0.30)	(743)
Both Experiments	(1,930)*	(1,416)	(650)	(850)	(0.55)	(0.30)	(870)
	1,733	1,648	450	775	0.53	0.30	1,095
	(1,733)	(969)	(800)	(1,073)	(0.40)	0.20	604

*These numbers differ from their two correspondents below since a slightly different set of computed-measured concentrations has been used. In fact, due to some missing σ_θ and $\Delta T/\Delta z$ values the three lines marked by an asterisk show computation results that did not use the entire data set used by the other two computations below, which do not require σ_θ and $\Delta T/\Delta z$ but only the Pasquill-Gifford stability.

3.2 GMAX Model Validation

Table 5 summarizes the principal statistical characteristics of such comparison. The numbers in parentheses in Table 5 allow some interesting comparison with two additional maximum ground-level concentration computation techniques. The lower numbers are the statistical performance results of the GMAX application without the Table 3 empirical correction of stability classification, while the upper numbers show the statistical performance results obtained using the G3D model.

3.3 Remarks on Gaussian Model Validation

It is surprising that simple corrections to the Pasquill-Gifford (insolation) method provide such a high increase in the performance of the Gaussian model for ground-level maximum concentration, a performance comparable (and, somehow, even better) than that of the Gaussian equation with ad hoc horizontal and vertical diffusion computations (and modifications). The main reason for this apparently strange behavior is that GMAX has been specifically calibrated for this type of computation (maximum ground-level concentration), while G3D has been evaluated to fit all concentration measurements. Thus, in spite of Table 5, G3D is still the best model to fit our three-dimensional SF_6 measurements.

The poor performance of the lower numbers between parentheses of Table 5 confirms, once again, that standard Gaussian model methodologies cannot be directly extrapolated, as a black box, to simulate simulate complex diffusion conditions such as coastal dispersion.

4. CONCLUSIONS

In spite of some large scatter in σ values, the Gaussian model validation can be considered successful. As expected at the beginning of this investigation, some stability adjustments were required, but this is a natural consequence of the different complex dispersion conditions that are encountered over large bodies of water and in the transition region at the shoreline.

Our mechanism for stability correction reflected in Tables 1 and 2 requires different modifications at different downwind distances. This can somehow limit the extendability of this approach to cases where the emission point is located at a distance much greater or much less than emission point of our experiments (about 3 to 5 miles from the shoreline).

However, we can say that the correction for the one-half mile offshore distance can be correctly extended to other cases (i.e., releases at more or less than 3 to 5 miles from the shoreline). In fact, from the release location to one-half mile offshore, diffusion is characterized only by turbulence conditions over the ocean, which can be assumed homogeneous and not yet affected by the shoreline instability (fumigation effect). We can therefore conclude that the first two columns of Tables 1 and 2 can be generally used to conservatively assess the impact at the shoreline of an offshore release. This is the most important case

since, with low level emissions, shoreline ground-level concentrations represent the maximum concentration impact, i.e., the most important parameter for regulatory applications.

If only ground-level maximum concentrations are of concern, as in most regulatory applications, GMAX provides a simpler methodology meeting this limited but important objective. In this case the stability conversion is simpler and does not depend upon downwind distance, therefore, facilitating the transferability of this approach. This method is accurate enough to be a first empirical screening technique for assessing the environmental impact of offshore emissions over a coastal area, showing that neutral to slightly stable conditions are the most appropriate ones to be used with standard Gaussian model application with PGT σ functions.

Care should be taken in applying the results presented in this paper to regions characterized by different meteorological and topographical features. Only future tracer studies will clarify the applicability of the empirical modifications proposed in this paper for treating the coastal diffusion processes.

ACKNOWLEDGEMENTS

Sincere appreciation is extended to Messrs. Robert Baxter and Vince Perun of AeroVironment Inc. for managing the study field work and the computer data analysis, respectively. This study has been sponsored by the Department of Interior, Bureau of Land Management under Contract No. AA851-CTO-56.

REFERENCES

Dahlquist, G. and A. Bjorck (1974): Numerical Methods. Prentice-Hall Inc., Englewood Cliffs, New Jersey.

DeMarrais, G.A. (1978): Atmospheric stability class determinations on a 481-meter tower in Oklahoma. Atmos. Environ. 12, 1957-1964.

Gifford, F.A. (1976): Turbulent diffusion-typing schemes: a review. Nuclear Safety 17, No. 1, 68-86.

Golder, P. (1968): Relations among stability parameters in the surface layer. Bound. Layer Meteor. 3, 47.

Hanna, S.R., G.A. Briggs, J. Deardorff, B.A. Egan, F.A. Gifford, and F. Pasquill (1977): AMS Workshop on Stability Classification Schemes and Sigma Curves -- Summary of Recommendations. Bull. Amer. Met. Soc. 58, No. 12, 1305-1309.

Kondo, J. (1975): Air-sea bulk transfer coefficients in diabatic conditions. Bound. Layer Meteor. 9, 91.

Schacher, G.E., K.L. Davidson, and C.W. Fairall: Atmospheric marine boundary layer convective mixing velocities in the California Coastal Region. Atmos. Environ. (to be published).

Skaggs, D.L. and E. Robinson (1976): A comparison of methods for estimating atmospheric stability and diffusion coefficients. JAPCA 26, No. 9, 888-891.

Taylor, G.I. (1921): Diffusion by continuous movements. Proc. London. Math. Soc., 20, 196.

U.S. Environmental Protection Agency (1980): Guideline on air quality models. Office of Air Quality Planning and Standards, Research Triangle Park, NC. Proposed Revisions, October.

Weil, J.C. (1979): Applicability of stability classification schemes and associated parameters to dispersion of tall stack plumes in Maryland. Atmos. Environ. 13, 819-831.

Zannetti, P., D. Wilbur, R. Baxter, and G. Schacher (1981): Southern California offshore air quality model validation study. AeroVironment Final Report AV-FR-81/559.

APPENDIX

A new scheme has been developed by the NPS for classifying atmospheric Pasquill stability for overwater regimes. This scheme uses the graphical relation between the Monin-Obukhov length, L, the roughness length, z_o, and the Pasquill classes proposed by Golder (1968). In this scheme, z_o is computed from the wind speed, as suggested by Kondo (1975), in the overwater regime, and L is computed using wind speed, air-sea temperature difference, ΔT, and relative humidity, applying an iterative computational algorithm (Schacher et al., in press).

From such z_o and L inputs, the Golder (1968) scheme gave, at each hour of our experiments, Pasquill stabilities in the range B-C-D. To improve our information, we divided each of these classes into three subclasses. For example, C was divided into C-, C, C+ where the - indicates the unstable side and + the stable side. This subdivision was simply performed by an empirical technique, dividing the B-C-D areas in the Golder (1968) graphical scheme into three appropriate subregions of nearly the same size.